

Experimental study of $pp\eta$ dynamics in the $pp \rightarrow pp\eta$ reaction*

P. Moskal^{1,2}, H.-H. Adam³, A. Budzanowski⁴, R. Czyżykiewicz², D. Grzonka¹, M. Janusz², L. Jarczyk², B. Kamys², A. Khoukaz³, K. Kilian¹, P. Kowina^{1,5}, K. Nakayama⁶, W. Oelert¹, C. Piskor-Ignatowicz², J. Przerwa², T. Rożek^{1,5}, R. Santo³, G. Schepers¹, T. Sefzick¹, M. Siemaszko⁵, J. Smyrski², S. Steltenkamp³, A. Täschner³, P. Winter¹, M. Wolke¹, P. Wüstner⁷, W. Zipper⁵

¹ *Institut für Kernphysik, Forschungszentrum Jülich, D-52425 Jülich, Germany*

² *Institute of Physics, Jagellonian University, PL-30-059 Cracow, Poland*

³ *Institut für Kernphysik, Westfälische Wilhelms-Universität, D-48149 Münster, Germany*

⁴ *Institute of Nuclear Physics, PL-31-342 Cracow, Poland*

⁵ *Institute of Physics, University of Silesia, PL-40-007 Katowice, Poland*

⁶ *Department of Physics and Astronomy, University of Georgia, Athens, GA 30602, USA and*

⁷ *Zentrallabor für Elektronik, Forschungszentrum Jülich, D-52425 Jülich, Germany*

(Dated: August 3, 2018)

A high statistics measurement of the $pp \rightarrow pp\eta$ reaction at an excess energy of $Q = 15.5$ MeV has been performed at the internal beam facility COSY-11. The stochastically cooled proton beam and the used detection system allowed to determine the momenta of the outgoing protons with a precision of 4 MeV/c (σ) in the center-of-mass frame. The determination of the four-momentum vectors of both outgoing protons allowed to derive the complete kinematical information of the $pp\eta$ -system. An unexpectedly large enhancement of the occupation density in the kinematical regions of low proton- η relative momenta is observed. A description taking the proton-proton and the η -proton interaction into account and assuming an on-shell incoherent pairwise interaction among the produced particles fails to explain this strong effect. Its understanding will require a rigorous three-body approach to the $pp\eta$ system and the precise determination of contributions from higher partial waves. We also present an invariant mass spectrum of the proton-proton system determined at $Q = 4.5$ MeV. Interestingly, the enhancement at large relative momenta between protons is visible also at such a small excess energy.

In contrast to all other determined angular distributions, the orientation of the emission plane with respect to the beam direction is extracted to be anisotropic.

PACS numbers: 13.60.Le; 13.75.-n; 13.85.Lg; 25.40.-h; 29.20.Dh

I. MANIFESTATION OF THE η -P-P INTERACTION

Due to the short live time of the flavour-neutral mesons (eg. π^0 , η , η'), the study of their interaction with nucleons or with other mesons is at present not feasible in direct scattering experiments. One of the methods permitting such investigations is the production of a meson in the nucleon-nucleon interaction close to the kinematical threshold or in kinematics regions where the outgoing particles possess small relative velocities. A mutual interaction among the outgoing particles manifests itself in the distributions of differential cross sections as well as in the magnitude and energy dependence of the total reaction rate.

In the last decade major experimental [1, 2, 3, 4, 5, 6, 7, 8] and theoretical [9, 10, 11, 12, 13] efforts were concentrated on the study of the creation of π^0 , η and η' mesons via the hadronic interactions [14, 15, 16]. Measurements have been performed in the vicinity of the kinematical threshold where only a few partial waves in both initial

and final state are expected to contribute to the production process. This simplifies significantly the interpretation of the data, yet still appears to be challenging due to the three particle final state system with a complex hadronic potential. The determined energy dependences of the total cross section for η' [1, 2] and η [2, 3, 4, 5, 6] mesons in proton-proton collisions are presented in figure 1. Comparing the data to the arbitrarily normalized phase-space integral (dashed lines) reveals that the proton-proton FSI enhances the total cross section by more than an order of magnitude for low excess energies. One recognizes also that in the case of the η' the data are described very well (solid line) assuming that the on-shell proton-proton amplitude exclusively determines the phase-space population. This indicates that the proton- η' interaction is too small to manifest itself in the excitation function within the presently achievable accuracy. In case of the η meson the increase of the total cross section for very low and very high energies is much larger than expected from the 1S_0 final state interaction between protons (solid line), though for both the $pp \rightarrow pp\eta$ and $pp \rightarrow pp\eta'$ reactions the dominance of the $^3P_0 \rightarrow ^1S_0s$ transition¹ is expected up to an excess energy of about

*We are very pleased to dedicate the present paper to Prof. Dr. Dr.h.c. Adam Strzałkowski on the occasion of his 80th birthday

¹ The transition between angular momentum combinations of the

40 MeV and 100 MeV, respectively [14]. The excess at higher energies can be assigned to the significant onset of higher partial waves, and the influence of the attractive interaction between the η meson and the proton could be a plausible explanation for the enhancement at threshold. A similar effect close to threshold is also observed in the photoproduction of η via the $\gamma d \rightarrow pn\eta$ reaction [19] indicating to some extent that the phenomenon is independent of the production process but rather related to the interaction among the η meson and nucleons in the $S_{11}(1535)$ resonance region. Indeed, a simple phenomenological treatment [13, 14, 21] – based on factorization of the transition amplitude into the constant primary production and the on-shell incoherent pairwise interaction among outgoing particles – describes very well the enhancement close to the threshold (dotted line). However, this approach fails for the description of the invariant mass distribution of the proton-proton and proton- η subsystems determined recently at $Q = 15$ MeV by the COSY-TOF collaboration [20]. The structure of this invariant mass distributions, which we confirm in this paper utilizing a fully different experimental method, may indicate a non-negligible contribution from the P-waves in the outgoing proton-proton subsystem [11]. These can be produced for instance via $^1S_0 \rightarrow ^3P_0s$ or $^1D_2 \rightarrow ^3P_2s$ transitions. This hypothesis encounters, however, difficulties in describing the excess energy dependence of the total cross section. The amount of the P-wave admixture derived from the proton-proton invariant mass distribution leads to a good description of the excitation function at higher excess energies while at the same time it spoils significantly the agreement with the data at low values of Q , as depicted by the dashed-dotted line in figure 1. However, these difficulties in reproducing the observed energy dependence might be due to the particular model used in reference [11], and thus higher partial wave contributions cannot a priori be excluded. In contrast to the P-wave contribution the three-body treatment [18] of the $pp\eta$ system (dashed-double-dotted line) leads to an even larger enhancement of the cross section near threshold than that based on the Ansatz of the factorization of the proton-proton and proton- η interactions. It must be kept in mind however that a too strong FSI effect predicted by the three-body model must be partially assigned to the neglect of the Coulomb repulsion in this preliminary

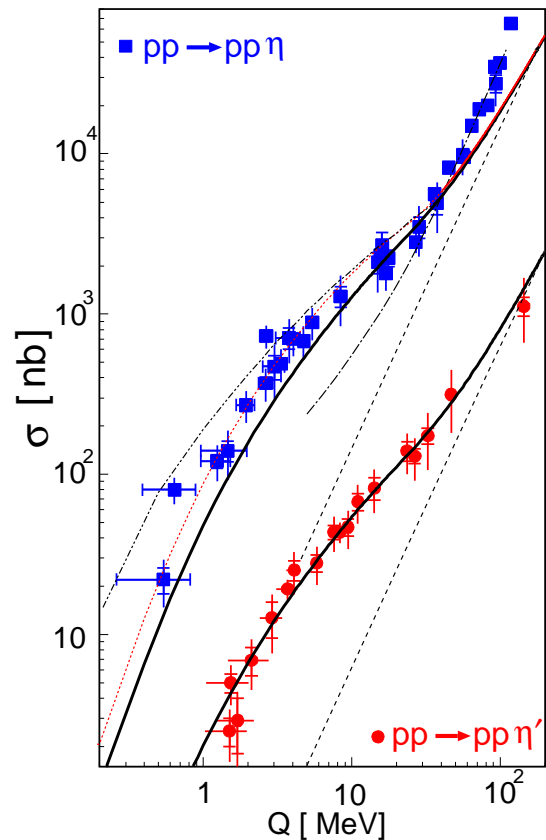


FIG. 1: Total cross section for the reactions $pp \rightarrow pp\eta'$ (circles) and $pp \rightarrow pp\eta$ (squares) as a function of the centre-of-mass excess energy Q . Data are from refs. [1, 2, 3, 4, 5, 6]. The dashed lines indicate a phase-space integral normalized arbitrarily.

The solid lines show the phase-space distribution with inclusion of the 1S_0 proton-proton strong and Coulomb interactions. In case of the $pp \rightarrow pp\eta$ reaction the solid line was fitted to the data in the excess energy range between 15 and 40 MeV. Additional inclusion of the proton- η interaction is indicated by the dotted line. The scattering length of $a_{p\eta} = 0.7 \text{ fm} + i0.4 \text{ fm}$ and the effective range parameter $r_{p\eta} = -1.50 \text{ fm} - i0.24 \text{ fm}$ [17] have been arbitrarily chosen. The dashed-dotted line represents the energy dependence taking into account the contribution from the $^3P_0 \rightarrow ^1S_0s$, $^1S_0 \rightarrow ^3P_0s$ and $^1D_2 \rightarrow ^3P_2s$ transitions [11]. Preliminary results for the $^3P_0 \rightarrow ^1S_0s$ transition with the full treatment of the three-body effects are shown as a dashed-double-dotted line [18]. The absolute scale of dashed-double-dotted line was arbitrary fitted to demonstrate the energy dependence only.

initial and final states are described according to the conventional notation [8] in the following way:

$$2S^i+1L_J^i \rightarrow 2S+1L_J, l \quad (1)$$

where, superscript "i" indicates the initial state quantities. S denotes the total spin of the nucleons, and J stands for the overall angular momentum of the system. L and l denote the relative angular momentum of the nucleon-nucleon pair and of the meson relative to the NN system, respectively. The values of orbital angular momenta are commonly expressed using the spectroscopic notation ($L = S, P, D, \dots$, and $l = s, p, d, \dots$).

calculations [18]. These illustrate that the simple phenomenological approach shown by the dotted line could fortuitously lead to the proper result, due to a mutual cancellation of the effects caused by the approximations assumed in calculations and the neglect of higher partial waves. This issue will be discussed further in section IV after the presentation of the new COSY-11 data. The above considerations show unambiguously that for the complete understanding of the low energy $pp\eta$ dynamics, in addition to the already established excitation function of the total cross section, a determination of the differential observables is also necessary. These will help

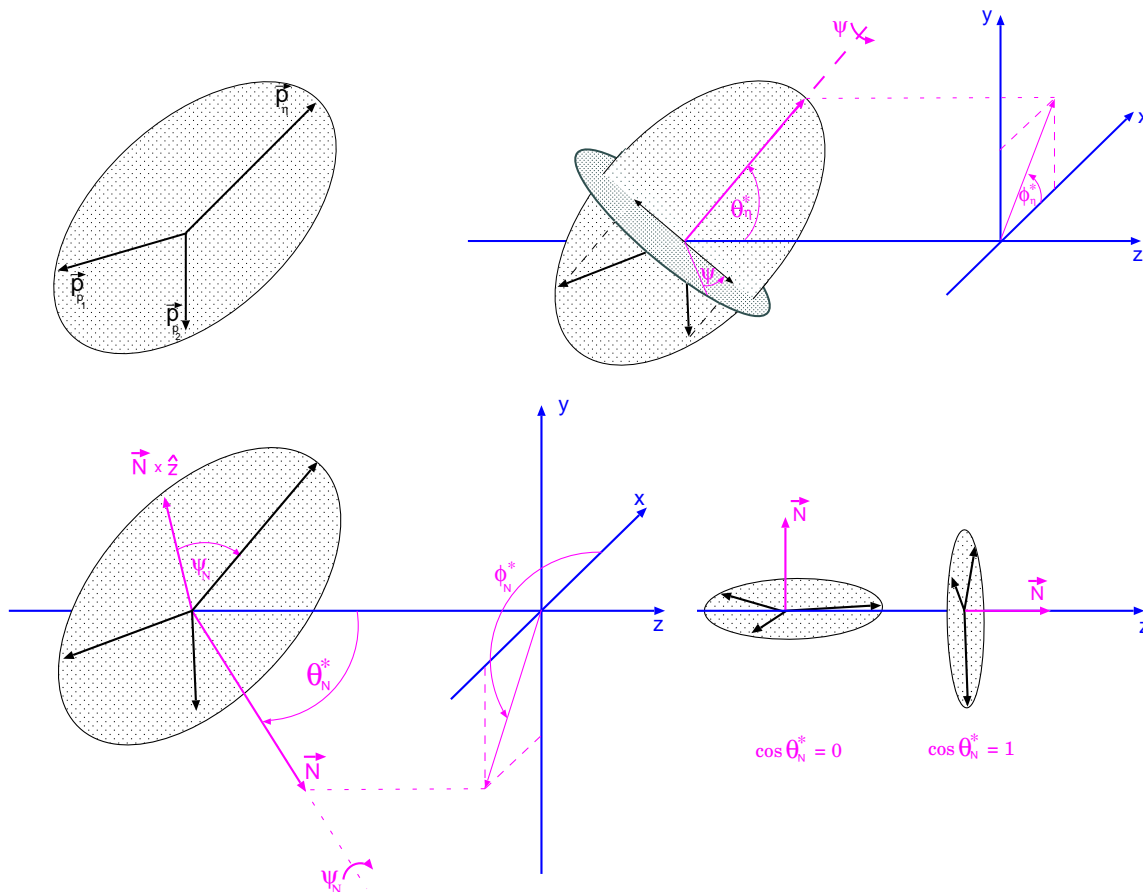


FIG. 2: Definition of the centre-of-mass kinematical variables used in this article for the description of the $pp\eta$ system. In the centre-of-mass system, the momenta of ejectiles lie in an emission plane. Within this plane the relative movement of the particles is fixed by the square of the invariant masses s_{pp} and $s_{p\eta}$. As remaining three variables needed to define the system uniquely we use either ϕ_η^* , θ_η^* , and ψ shown in the upper panel or ϕ_N^* , θ_N^* , and ψ_N defined in the lower panel. \vec{N} is a vector normal to the emission plane, which can be calculated as the vector product of the centre-of-mass momentum vectors of the outgoing protons. As an example two extreme orientations of the emission plane are shown in the right-lower panel. For further descriptions see the text.

to disentangle effects caused by the proton- η interaction and the contributions from higher partial waves. In this article we present distributions determined experimentally for two sets of orthogonal variables fully describing the $pp\eta$ system, which was produced at an excess energy of $Q = 15.5$ MeV via the $pp \rightarrow pp\eta$ reaction using the COSY-11 [22, 23] facility at COSY [24].

II. CHOICE OF OBSERVABLES

For the full description of the three particle system five independent variables are required. In the center-of-mass frame, due to the momentum conservation, the momentum vectors of the particles are lying in one plane often referred to as the emission, reaction or decay plane. In this plane (depicted in figure 2) a relative movement of the particles can be described by two variables only. The square of the invariant masses of the di-proton and proton- η system denoted as s_{pp} and $s_{p\eta}$, respectively,

constitute a natural choice for the study of the interaction within the $pp\eta$ system. This is because in the case of non-interacting objects the surface spanned by these variables is homogeneously populated. The interaction among the particles modifies that occupation density and in consequence facilitates an easy qualitative interpretation of the experimental results.

The remaining three variables must define an absolute orientation of the emission plane in the distinguished coordinate system. This may be realized for example by defining the orientation for the momentum of the arbitrarily chosen particle in the center-of-mass frame and the angle which describes the rotation around the direction fixed by that particle. In one of our choices made following reference [25, 26] the corresponding variables are the polar and the azimuthal angle of the η momentum vector, depicted in figure 2 as ϕ_η^* and θ_η^* , respectively, and the angle ψ describing the rotation around the direction established by the momentum of the η meson. Figure 2 demonstrates that such rotation neither affects

the η meson momentum nor changes the configuration of the momenta in the emission plane. In the case of experiments with unpolarized beams and targets the only favoured direction is that of the beam line. Therefore, as a zero value of the ψ angle we have chosen the projection of the beam direction on the plane perpendicular to the momentum vector of the η meson. Note that we identify the z-axis with the beam direction. The ϕ_η^* , θ_η^* and ψ variables can also be interpreted as Euler angles allowing for the rotation of the emission plane into a xz-plane.

As a second possibility we will describe an orientation of the emission plane by the azimuthal- and polar angle of the vector normal to that plane [27]. These angles are shown in figure 2 as ϕ_N^* and θ_N^* , respectively. Further the absolute orientation of the particles momenta in the emission plane will be described by ψ_N , the angle between η meson and the vector product of the beam momentum and the vector \vec{N} .

Obviously, the interaction between the particles does not depend on the orientation of the emission plane, and therefore, it will fully manifest itself in the occupation density of the Dalitz plot which in our case will be represented in terms of the square of the invariant masses of the two particle subsystems. The distribution of the orientation of the emission plane will reflect, however, the correlation between the initial and final channel and hence its determination should be helpful for the investigation of the production mechanism.

III. EXPERIMENT AND DATA ANALYSIS

Using the COSY-11 detection system [22, 23], utilizing a stochastically cooled proton beam of the cooler synchrotron COSY [24] and a hydrogen cluster target [28], we have performed a high statistics measurement of the $pp \rightarrow pp\eta$ reaction at a nominal beam momentum of 2.027 GeV/c. The experiment was based on the four-momentum registration of both outgoing protons, whereas the η meson was identified via the missing mass technique. The positively charged particles have been identified combining the time of flight between the S1 and S3 scintillation detectors and the momentum reconstructed by tracking trajectories registered by means of the drift chambers back to the target. The detection setup is sketched in figure 3.

The accuracy of the missing mass reconstruction depends on two parameters: the spread of the beam momentum as well as the precision of the measured momenta of the outgoing protons. The latter is predominantly due to the geometrical spread of the beam. Since for the reconstruction of the momenta we assume that the reaction takes place in the middle of the target we cannot correct on an event-by-event basis for the momentary spread of the beam. However, we can rectify the smearing due to the shifts of the centre of the beam relative to the target as well as the average changes of the absolute beam momentum during the experiment. There-

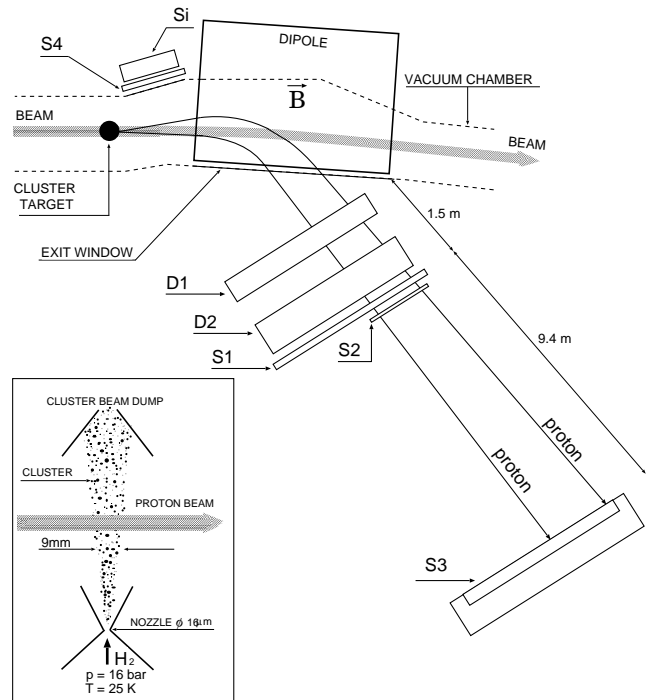


FIG. 3: Schematic view of the COSY-11 detection setup [22]. The cluster target [28] is located in front of the accelerator dipole magnet. Positively charged particles which leave the scattering chamber through the thin exit foil are detected in two drift chamber stacks D1, D2 and in the scintillator hodoscopes S1, S2 and S3. Scintillation detector S4 and the position sensitive silicon pad detector Si are used in coincidence with the S1 counter for the registration of the elastically scattered protons. Elastic scattering is used for an absolute normalisation of the cross sections of the investigated reactions and for monitoring both the geometrical spread of the proton beam and the position at which beam crosses the target [23]. In the left-lower corner a schematic view of the interaction region is depicted.

fore, after the selection of events with two registered protons, as a first step of the more refined analysis the data were corrected for the mean beam momentum changes (see fig. 4) determined from the measured Schottky frequency spectra and the known beam optics. In a next step, from the distributions of the elastically scattered protons, the Schottky frequency spectrum, and the missing mass distribution of the $pp \rightarrow ppX$ reaction, we have estimated that the spread of the beam momentum, and the spread of the reaction points in horizontal and vertical direction amount to $\sigma(p_{beam}) = 0.63 \pm 0.03$ MeV/c, $\sigma(x) = 0.22 \pm 0.02$ cm, and $\sigma(y) = 0.38 \pm 0.04$ cm, respectively. Details of this procedure can be found in references [23, 29]. Further on, a comparison of the experimentally determined momentum spectra of the elastically scattered protons with the distributions simulated with different beam and target conditions allows us to establish the position at which the centre of the beam crosses the target with an accuracy of 0.25 mm [23]. Accounting for the movement of the beam relative to the target we improved the missing mass resolution as demonstrated in

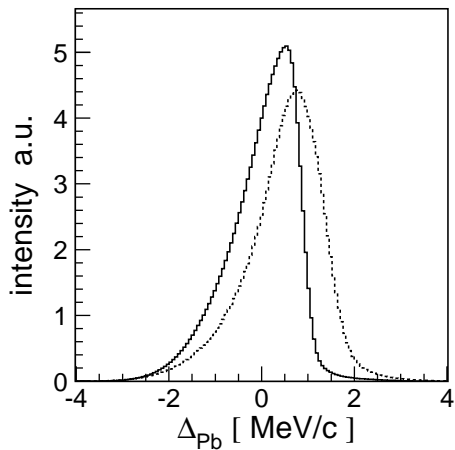


FIG. 4: The dashed curve denotes the proton beam momentum distribution integrated over the whole measurement period. On the horizontal scale, the value of zero is set at a nominal beam momentum equal to 2.027 GeV/c. The solid line shows the beam momentum distribution after the correction for the mean value which was determined in 10 second intervals.

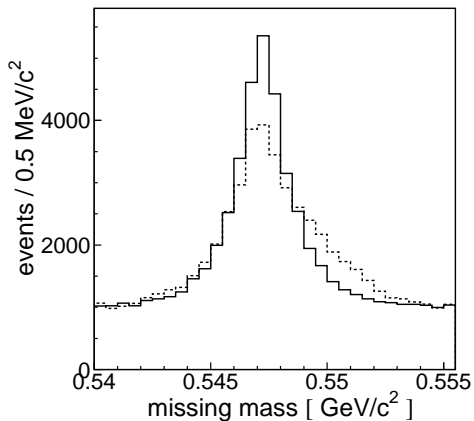


FIG. 5: Missing mass distribution for the $pp \rightarrow ppX$ reaction determined by means of the COSY-11 detection system at a beam momentum of 2.027 GeV. The solid histogram presents the data corrected for effects of the time dependent relative shifts between the beam and the target using the method described in reference [23]. The dashed histogram shows the result before the correction.

figure 5. After this betterment, the peak originating from the $pp \rightarrow pp\eta$ reaction became more symmetric and the signal to background ratio increased significantly. The background was simulated taking into account $pp \rightarrow ppX$ reactions with $X = 2\pi, 3\pi$ and 4π . Since we consider here only the very edge of the phase space distribution where the protons are produced predominantly in the S-wave the shape of the background can be reproduced assuming that the homogenous phase space distribution is modified only by the interaction between protons. Indeed, as can be observed in figure 6 the simulation describes the data very well. The calculated spectrum is hardly distinguishable from the experimental points.

The position of the peak on the missing mass spectrum and the known mass of the η meson [30] enabled

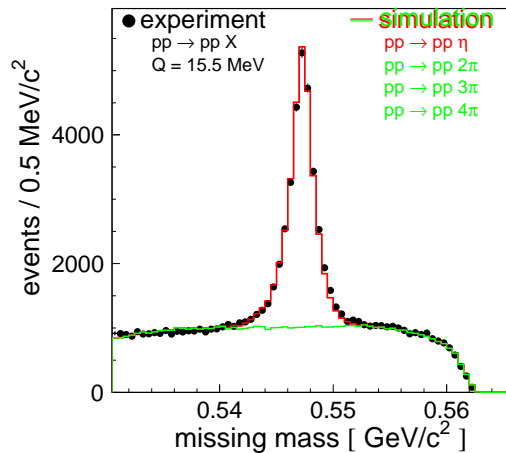


FIG. 6: Missing mass spectrum for the $pp \rightarrow ppX$ reaction determined in the experiment at a beam momentum of 2.0259 GeV/c. The mass resolution amounts to 1 MeV/c²(σ). The superimposed histograms present the simulation for $1.5 \cdot 10^8$ events of the $pp \rightarrow pp\eta$ reaction, and 10^{10} events for the reactions $pp \rightarrow pp2\pi$, $pp \rightarrow pp3\pi$ and $pp \rightarrow pp4\pi$. The simulated histograms were fitted to the data varying only the magnitude. The fit resulted in 24009 ± 210 events with the production of the η meson.

to determine the actual absolute beam momentum to be $p_{beam} = 2.0259 \text{ GeV/c} \pm 0.0013 \text{ GeV/c}$, which agrees within error limits with the nominal value of $p_{beam}^{nominal} = 2.027 \text{ GeV/c}$. The real beam momentum corresponds to the excess energy of the $pp\eta$ system equal to $Q = 15.5 \pm 0.4 \text{ MeV}$.

A. Covariance matrix and kinematical fitting

As already mentioned in the previous section at the COSY-11 facility the identification of the $pp \rightarrow pp\eta$ reaction is based on the measurement of the momentum vectors of the outgoing protons and the utilisation of the missing mass technique. Inaccuracy of the momentum determination manifests itself in the population of kinematically forbidden regions of the phase space, preventing a precise comparison of the theoretically derived and experimentally determined differential cross sections. Figure 7 visualizes this effect and clearly demonstrates that the data scatter significantly outside the kinematically allowed region (solid line), in spite of the fact that the precision of the fractional momentum determination in the laboratory system ($\sigma(p_{lab})/p_{lab} \approx 7 \cdot 10^{-3}$) is quite high. Therefore, when seeking for small effects like for example the influence of the proton- η interaction on the population density of the phase-space, one needs either to fold theoretical calculations with the experimental resolution, or to perform the kinematical fitting of the data. Both procedures require the knowledge of the covariance matrix, and thus its determination constitutes a necessary step in the differential analysis and interpretation of the data.

In order to derive the covariance matrix we need to

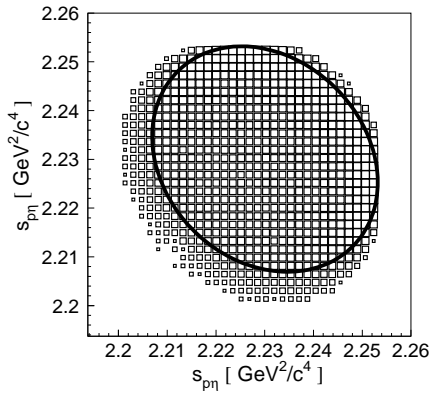


FIG. 7: Dalitz plot distribution of the $pp \rightarrow pp\eta$ reaction simulated at $Q = 15.5$ MeV. The number of entries is shown in a logarithmic scale. The solid line gives the kinematically allowed area. The result was obtained taking into account the experimental conditions as described in the text.

recognize and quantify all possible sources of errors in the reconstruction of the two proton momenta \vec{p}_1 and \vec{p}_2 . The four dominant effects are: i) finite distributions of the beam momentum and of the reaction points, ii) multiple scattering in the dipole chamber exit foil, air, and detectors, iii) finite resolution of the position determination of the drift chambers, and iv) a possible inadequate assignment of hits to the particle tracks in drift chambers in the case of very close tracks. Some of these, like the multiple scattering, depend on the outgoing protons' momenta, others, like the beam momentum distribution, depend on the specific run conditions and therefore must be determined for each run separately.

In order to estimate the variances and covariances for all possible combinations of the momentum components of two registered protons we have generated $1.5 \cdot 10^8$ $pp \rightarrow pp\eta$ events and simulated the response of the COSY-11 detection setup taking into account the above listed factors and the known resolutions of the detector components. Next, we analysed the signals by means of the same reconstruction procedure as used in case of the experimental data. Covariances between the i^{th} and the j^{th} components of the event vector ($P = [p_{1x}, p_{1y}, p_{1z}, p_{2x}, p_{2y}, p_{2z}]$) were established as the average of the product of the deviations between the reconstructed and generated values. The explicit formula for the sample of N reconstructed events reads:

$$cov(i, j) = \frac{1}{N} \sum_{k=1}^N (P_{i,gen}^k - P_{i,recon}^k)(P_{j,gen}^k - P_{j,recon}^k),$$

where $P_{i,gen}^k$ and $P_{i,recon}^k$ denote the generated and reconstructed values for the i^{th} component of the vector P describing the k^{th} event.

Because of the inherent symmetries of the covariance matrix ($cov(i, j) = cov(j, i)$) and the indistinguishability

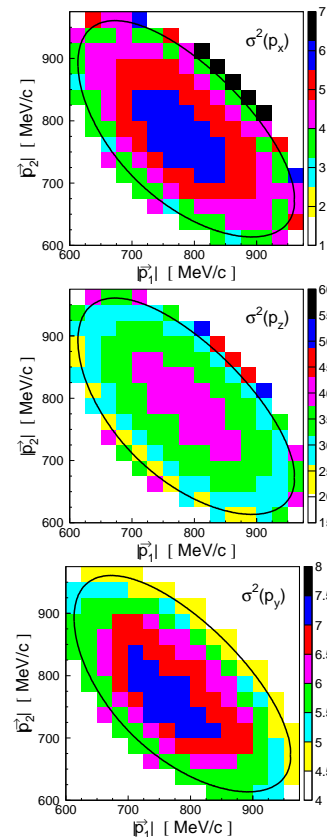


FIG. 8: Variances of the protons's momentum components $\sigma^2(p_x)$, $\sigma^2(p_z)$, and $\sigma^2(p_y)$ shown as a function of the absolute values of the measured momenta.

of the registered protons² there are only 12 independent values which determine the 6 x 6 error matrix V unambiguously.

Since inaccuracies of the momentum determination depend on the particle momentum itself (eg. multiple scattering) and on the relative momentum between protons (eg. trajectories reconstruction from signals in drift chambers), we have determined the covariance matrices as a function of the absolute momentum of both protons: $cov(i, j, |\vec{p}_1|, |\vec{p}_2|)$.

As an example we present the covariance matrix for the mean values of $|\vec{p}_1|$ and $|\vec{p}_2|$ in units of MeV^2/c^2 , as established in the laboratory system with the z -coordinate parallel to the beam axis and y -coordinate corresponding to the vertical direction.

$$V = \begin{bmatrix} p_{1x} & p_{1y} & p_{1z} & p_{2x} & p_{2y} & p_{2z} \\ 5.6 & 0.0 & -13.7 & 1.7 & 0.1 & -3.0 \\ - & 7.1 & 0.1 & - & -0.2 & -0.2 \\ - & - & 37.0 & - & - & 5.4 \\ - & - & - & - & - & - \\ - & - & - & - & - & - \\ - & - & - & - & - & - \end{bmatrix} \begin{matrix} p_{1x} \\ p_{1y} \\ p_{1z} \\ p_{2x} \\ p_{2y} \\ p_{2z} \end{matrix} \quad (2)$$

² The symmetry of all observables under the exchange of the two protons ($\vec{p}_1 \leftrightarrow \vec{p}_2$) implies that $cov(i, j) = cov(i \pm 3, j \pm 3)$, where the '+' has to be taken for $i, j = 1, 2, 3$ and the '-' for $i, j = 4, 5, 6$. Thus for example $cov(2, 4) = cov(5, 1)$.

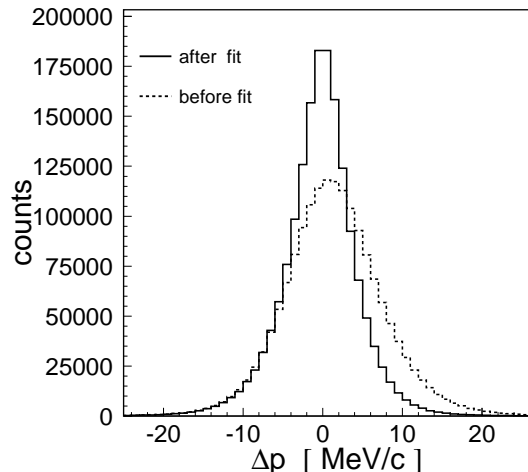


FIG. 9: Spectrum of differences between generated and – after simulation of the detector response – reconstructed absolute momenta of protons, as determined before (dashed line) and after the kinematical fit (solid line).

The picture shows results obtained taking into account the experimental conditions as described in the text.

Since the measurements have been performed close to the kinematical threshold the ejectile momentum component parallel to the beam is by far the largest one and its variance ($var(p_z) = 37 \text{ MeV}^2/c^2$) determines in first order the error of the momentum measurement. The second largest contribution stems from an anti-correlation between the x - and z - momentum components ($cov(p_x, p_z) = -13.7 \text{ MeV}^2/c^2$), which is due to the bending of the proton trajectory – mainly in the horizontal direction – inside the COSY-11 dipole magnet (see fig. 3). There is also a significant correlation between the z components of different protons which is due to the smearing of the reaction points, namely, if in the analysis the assumed reaction point differs from the actual one, a mistake made in the reconstruction affects both protons similarly. Figure 8 depicts the variation of $var(p_x)$, $var(p_y)$, and $var(p_z)$ over the momentum plane ($|\vec{p}_1|$, $|\vec{p}_2|$). Taking into account components of the covariance matrices $V(|\vec{p}_1|, |\vec{p}_2|)$ and the distribution of the proton momenta for the $pp \rightarrow pp\eta$ reaction at $Q = 15.5 \text{ MeV}$ results in an average error for the measurement of the proton momentum of about $6 \text{ MeV}/c$. This can be also deduced from the distribution of the difference between the generated and reconstructed absolute momenta of the protons. The corresponding spectrum is plotted as a dashed line in figure 9.

In the experiment we have measured 6 variables and once we assume that the event corresponds to the $pp \rightarrow pp\eta$ reaction only 5 of them are independent. Thus we have varied the values of the event components demanding that the missing mass is equal to the mass of the η meson and we have chosen that vector which was the closest to the experimental one. The inverse of the covariance matrix was used as a metric for the distance

calculation. The kinematical fit improves the resolution by a factor of about 1.5 as can be concluded from comparing the dashed- and solid lines in figure 9. The finally resulting error of the momentum determination amounts to $4 \text{ MeV}/c$.

B. Multidimensional acceptance corrections and results

At the excess energy of $Q = 15.5 \text{ MeV}$ the COSY-11 detection system does not cover the full 4π solid angle in the centre-of-mass system of the $pp \rightarrow pp\eta$ reaction. Therefore, the detailed study of differential cross sections requires corrections for the acceptance. Generally, the acceptance should be expressed as a function of the full set of mutually orthogonal variables which describe the studied reaction unambiguously. As introduced in section II, to define the relative movement of the particles in the reaction plane we have chosen two squares of the invariant masses: s_{pp} and $s_{p\eta}$, and to define the orientation of this plane in the center-of-mass frame we have

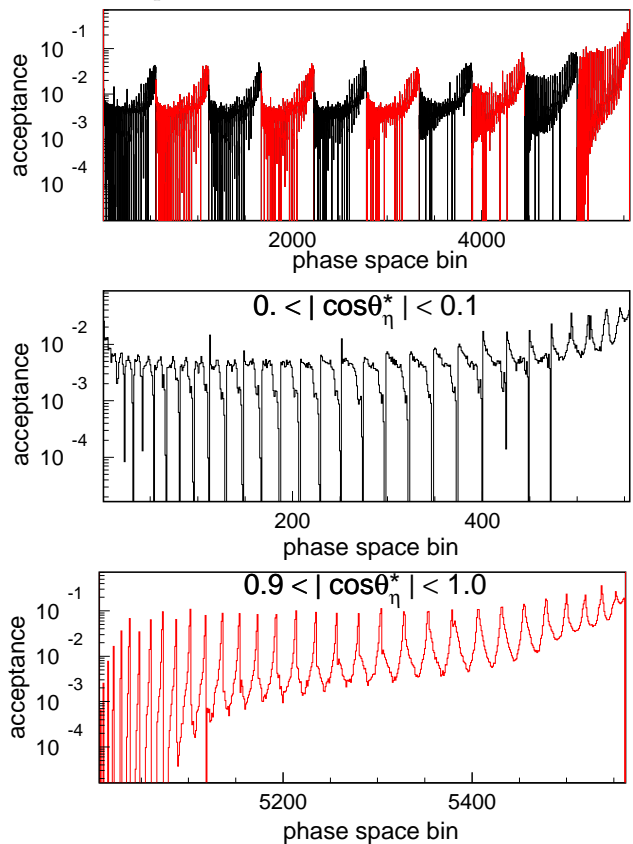


FIG. 10: Acceptance of the COSY-11 detection system for the $pp \rightarrow pp\eta$ reaction at an excess energy of $Q = 15.5 \text{ MeV}$ presented as a function of $s_{pp}, s_{p\eta}$, and $|\cos(\theta_\eta^*)|$. The numbers were assigned to the bins in the three dimensional space $s_{pp} - s_{p\eta} - |\cos(\theta_\eta^*)|$ by first incrementing the index of s_{pp} next of $s_{p\eta}$ and on the end that of $|\cos(\theta_\eta^*)|$. Partitioning of $|\cos(\theta_\eta^*)|$ into ten bins is easily recognizable. The two lower pictures show the acceptance for the first and the last bin of $|\cos(\theta_\eta^*)|$.

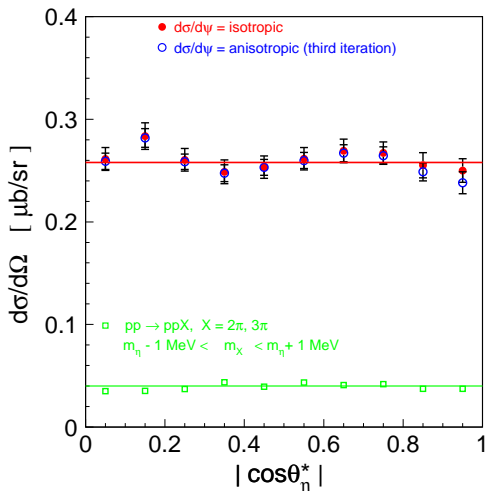


FIG. 11: Distribution of the polar angle of the emission of the η meson in the centre-of-mass system. Experimental data were corrected for the acceptance in the three dimensional space (s_{pp} , $s_{p\eta}$, $|\cos(\theta_\eta^*)|$). Full circles show the result with the assumption that the distribution of the ψ angle is isotropic, and the open circles are extracted under the assumption that $\frac{d\sigma}{d\psi}$ is as derived from the data (see text). Both results have been normalized to each other in magnitude.

Open squares show (in arbitrary units) the distribution of the multi-pion production for the invariant mass of the pions ranging between ± 1 MeV around the mass of the η meson.

taken the three Euler angles: The first two are simply the polar ϕ_η^* and azimuthal θ_η^* angles of the momentum of the η meson and the third angle ψ describes the rotation of the reaction plane around the axis defined by the momentum vector of the η meson. In the data evaluation we considerably benefit from the basic geometrical symmetries satisfied by the $pp \rightarrow pp\eta$ reaction. Due to the axial symmetry of the initial channel of the two unpolarized colliding protons the event distribution over ϕ_η^* must be isotropic. Thus, we can safely integrate over ϕ_η^* , ignoring that variable in the analysis. Furthermore, taking advantage of the symmetry due to the two identical particles in the initial channel, without losing the generality, we can express the acceptance as a function of s_{pp} , $s_{p\eta}$, $|\cos(\theta_\eta^*)|$, and ψ . To facilitate the calculations we have divided the range of $|\cos(\theta_\eta^*)|$ and ψ into 10 bins and both s_{pp} and $s_{p\eta}$ into 40 bins each. In the case of the s_{pp} and $s_{p\eta}$ the choice was made such that the width of the interval corresponds to the standard deviation of the experimental accuracy. For $|\cos(\theta_\eta^*)|$ and ψ we have taken only ten partitions since from the previous experiments we expect only a small variation of the cross section over these variables [20, 26, 37]. In this representation, however, the COSY-11 detection system covers only 50% of the phase-space for the $pp \rightarrow pp\eta$ reaction at $Q = 15.5$ MeV. To proceed with the analysis we assumed that the distribution over the angle ψ is isotropic as it was for example experimentally determined for the $pp \rightarrow pp\omega$, $pp \rightarrow pp\rho$, or $pp \rightarrow pp\phi$ reactions [25, 26]. Please note that this is the only assumption of the reaction dynamics performed in the present evaluation. The validity of this supposition in the case of the $pp \rightarrow pp\eta$ reaction will be discussed later.

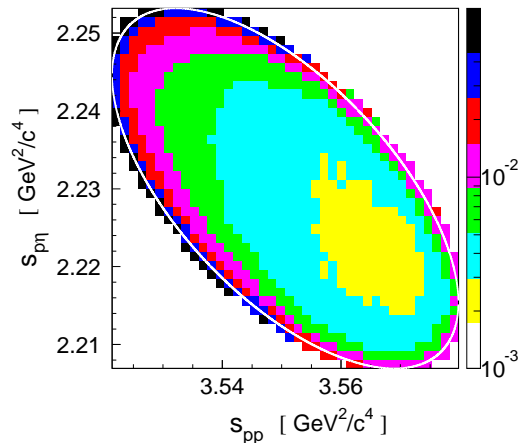


FIG. 12: COSY-11 detection acceptance as a function of s_{pp} and $s_{p\eta}$, calculated under the assumption that the differential cross sections $\frac{d\sigma}{d\cos(\theta_\eta^*)}$ and $\frac{d\sigma}{d\psi}$ are isotropic.

In the calculations we exploit also the symmetry of the cross sections under the exchange of the two identical particles in the final state which reads: $\sigma(s_{p_1\eta}, \psi) = \sigma(s_{p_2\eta}, \psi + \pi)$. The resultant acceptance is shown in figure 10. One recognizes that only a small part (3%) of the phase-space is not covered by the detection system. In further calculations these holes were corrected according to the assumption of a homogeneous phase space distribution. Additionally it was checked that the corrections under other suppositions eg. regarding also the proton-proton FSI leads to negligible differences. Full points in figure 11 present the distribution of the polar angle of the η meson as derived from the data after the acceptance correction. Within the statistical accuracy it is isotropic. Taking into account this angular distribution of the cross section we can calculate the acceptance as a function of s_{pp} and $s_{p\eta}$ only. This is shown in figure 12, where one sees that now the full phase space is covered. This allows us to determine the distributions of s_{pp} and $s_{p\eta}$. The correctness of the performed procedures for the simulation of the detectors response, the event reconstruction programs, the kinematical fitting and acceptance correction can be confirmed by comparing the distribution generated (figure 13a) with the ones which underwent the complete analysis chain described in this section (figure 13b).

Knowing the distribution of the polar angle of the η meson θ_η^* and those for the invariant masses s_{pp} and $s_{p\eta}$ we can check whether the assumption of the isotropy of the cross section distribution versus the third Euler's angle ψ is corroborated by the data. For that purpose we calculated the acceptance as a function of ψ and $s_{p\eta}$ assuming the shape of the differential cross sections of $\frac{d\sigma}{ds_{pp}}$ and $\frac{d\sigma}{d\cos(\theta_\eta^*)}$ as determined experimentally. The obtained $\frac{d\sigma}{d\psi}$ distribution is shown in figure 14 and is not isotropic as assumed at the beginning. A fit of the function of the form $\frac{d\sigma}{d\psi} = a + b \cdot |\sin(\psi)|$ gives the value of $b = 0.079 \pm 0.014 \mu\text{b}/\text{sr}$, indeed significantly different from the isotropic solution. This deviation cannot be

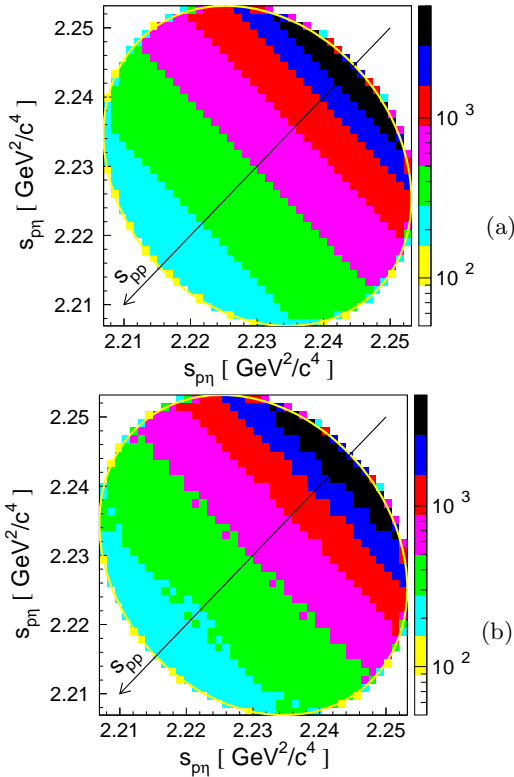


FIG. 13: (a) Dalitz plot distribution simulated for the $pp \rightarrow pp\eta$ reaction at $Q = 15.5$ MeV. In the calculations the interaction between protons was taken into account. (b) Dalitz plot distribution reconstructed from the COSY-11 detector response simulated for events from figure (a) taking into account the smearing of the beam and target, multiple scattering in the materials, and the detectors resolution. The evaluation included momentum reconstruction, kinematical fitting and the acceptance correction exactly in the same way as performed for the experimental data. The lines surrounding the Dalitz plots depict the kinematical limits.

assigned to any unknown behaviour of the background since the obtained distribution can be regarded as background free. This is because the number of $pp \rightarrow pp\eta$ events was elaborated for each invariant mass interval separately. The exemplarily missing mass spectra for the first, fourth, seventh and tenth interval of ψ values, corrected for the acceptance are presented in figure 15.

From this figure one can infer that the shape of the background is well reproduced not only for the overall missing mass spectrum as shown previously in figure 6 but also locally in each region of the phase space. Since the experimental data are quite well described by the simulations we can rather exclude the possibility of a significant systematical error which could cause the observed anisotropy of the differential cross section $\frac{d\sigma}{d\psi}$.

The evaluated distribution is however in disagreement with our working assumption that the $\sigma(\psi)$ is isotropic. Therefore we performed a full acceptance correction procedure from the very beginning assuming that the distribution of $\frac{d\sigma}{d\psi}$ is as determined from the data. After

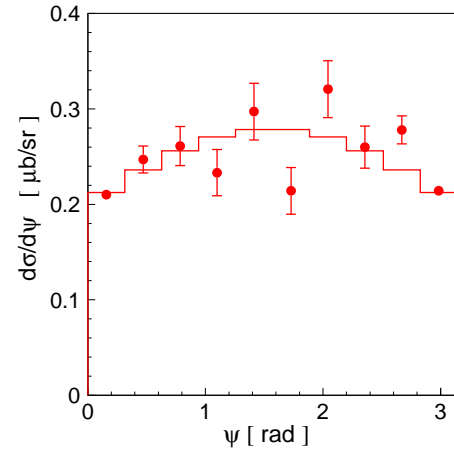


FIG. 14: Distribution of the cross section as a function of the angle ψ as determined in the first iteration. The superimposed histogram corresponds to the fit of the function $\frac{d\sigma}{d\psi} = a + b \cdot |\sin(\psi)|$. The range of the ψ angle is shown from 0 to π only, since in the analysis we take advantage of the symmetry $\frac{d\sigma}{d\psi}(\psi) = \frac{d\sigma}{d\psi}(\psi + \pi)$.

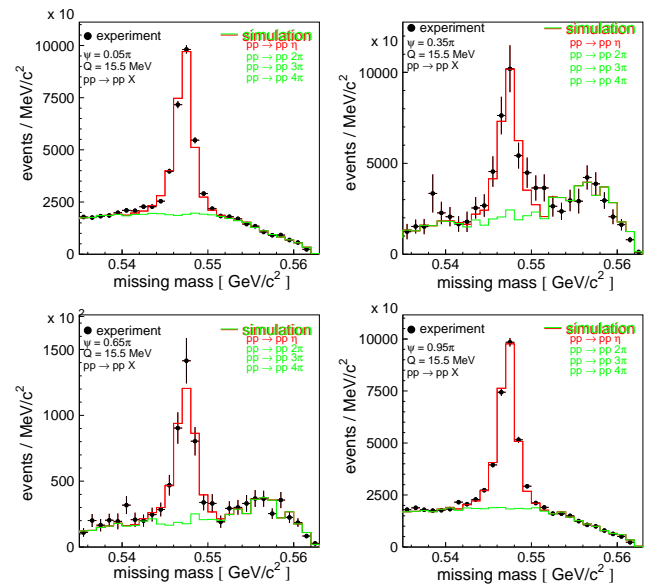


FIG. 15: Missing mass distributions for the first, fourth, seventh and tenth bin of ψ with the superimposed lines from the simulation of $pp \rightarrow pp\eta$ and the multi-pion background $pp \rightarrow pp(m\pi)$ reactions. Amplitudes of simulated distributions were fitted to the experimental points.

repeating the procedure three times we observed that the input and resultant distributions are in good agreement. The result after the third iteration is shown in figure 16 by the full circles. It is only slightly different from the one obtained after the first iteration as shown in figure 14. To rise the confidence of the convergence of the performed iteration we accomplished the full procedure once more, but now assuming that the distribution of $\frac{d\sigma}{d\psi}$ is much more anisotropic than determined from the data. As an entry distribution we took the dashed line shown in figure 16. Again after two iterations we have got the same result as before. Finally determined values

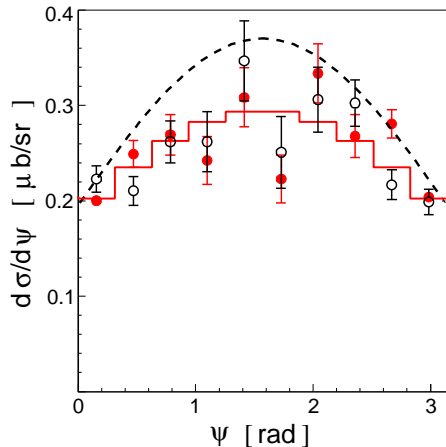


FIG. 16: Distribution of the cross section as a function of the angle ψ . Full circles stand for the final results of the $\frac{d\sigma}{d\psi}$ obtained after three iterations. The superimposed histogram (solid line) corresponds to the fit of the function $\frac{d\sigma}{d\psi} = a + b \cdot |\sin(\psi)|$ which resulted in $a = 0.186 \pm 0.004 \mu\text{b/sr}$ and $b = 0.110 \pm 0.014 \mu\text{b/sr}$. The dashed line shows the entry distribution used for the second series of iterations as described in the text.

Open circles represent the data from the left upper corner of the Dalitz plot (see for example figure 12). At that region of the Dalitz plot due to the non-zero four dimensional acceptance over $(s_{pp}, s_{p\eta}, |\cos(\theta_\eta^*)|, \psi)$ bins the spectrum (open circles) was corrected without a necessity of any assumptions concerning the reaction cross section.

TABLE I: Differential cross section in the ψ angle for the $pp \rightarrow pp\eta$ reaction at $Q = 15.5$ MeV. Fitting to the data a function of the form $\frac{d\sigma}{d\psi} = a + b |\sin(\psi)|$ resulted in $a = 0.186 \pm 0.004 \mu\text{b/sr}$ and $b = 0.110 \pm 0.014 \mu\text{b/sr}$. Figure 16 illustrates the result.

$\psi[\text{rad}]$	$\frac{d\sigma}{d\psi} \left[\frac{\mu\text{b}}{\text{rad}} \right]$ experiment	$\frac{d\sigma}{d\psi} \left[\frac{\mu\text{b}}{\text{rad}} \right]$ fit
0.157	0.200 ± 0.004	0.202
0.471	0.249 ± 0.014	0.235
0.785	0.269 ± 0.021	0.263
1.100	0.242 ± 0.025	0.283
1.414	0.309 ± 0.031	0.294
1.728	0.223 ± 0.025	0.294
2.042	0.334 ± 0.031	0.283
2.356	0.268 ± 0.023	0.263
2.670	0.281 ± 0.015	0.235
2.985	0.204 ± 0.004	0.202

for $\frac{d\sigma}{d\psi}(\psi)$ are given in table I. To corroborate this observation we have evaluated the distribution over ψ angle (see figure 16) from the phase space region which has no holes in the acceptance expressed as a four-dimensional function of the variables s_{pp} , $s_{p\eta}$, $|\cos(\theta_\eta^*)|$, and ψ , this is for the values of s_{pp} and $s_{p\eta}$ corresponding to the upper left corner of figure 12. Again the obtained distribution presented as open circles in figure 16 is anisotropic, and moreover agrees with the spectrum determined from all events. The anisotropy of the cross section in the ψ an-

gle reflects itself in an anisotropy of the orientation of the emission plane.

The determined cross section distribution in function of the polar angle θ_N^* of the vector normal to that plane is shown in figure 17 and the corresponding values are listed in table II. The distribution is not isotropic, which

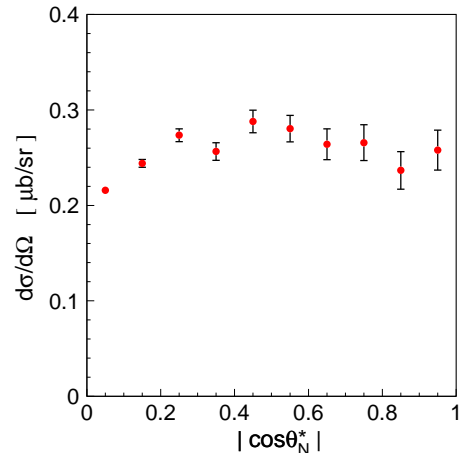


FIG. 17: Differential cross section as a function of the polar angle of the vector normal to the emission plane.

is particularly visible for the low values of $|\cos(\theta_N^*)|$ burdened with small errors. As depicted in figure 2 the $|\cos(\theta_N^*)| = 0$ denotes such configuration of the ejectiles momenta in which the emission plane comprises the beam axis. In that case the acceptance of the COSY-11 detection system is much larger than for the configuration where the emission plane is perpendicular to the beam. Due to this reason the error bars in figure 17 increase with growth of $|\cos(\theta_N^*)|$. It is worth to stress that the tendency of the $pp\eta$ system to be produced preferentially if the emission plane is perpendicular to the beam is in line with the preliminary analysis of the experiment performed by the TOF collaboration [27]. Elucidation of that non-trivial behaviour can reveal interesting features of the dynamics of the production process.

It is important to note that the shape of the s_{pp} , $s_{p\eta}$, and $\cos(\theta_\eta^*)$ distributions keeps unchanged during the whole iteration procedure. Figure 18 shows the distributions of the square of the proton-proton and proton- η invariant masses. The spectra after the second and third iterations are shown. One recognizes that the form of the spectra remains unaltered. The same conclusion can be drawn for the $\frac{d\sigma}{d|\cos(\theta_\eta^*)|}$ distribution as demonstrated in figure 11. From that comparison one can conclude that the shapes of the determined distributions are – within the statistical accuracy – independent of the shape of the $\frac{d\sigma}{d\psi}$ cross section and can be treated as derived in a completely model independent manner. Similarly, as in the case of the $\frac{d\sigma}{d\psi}$ distribution, the differential cross sections in all other variables reported in this article are not deteriorated by the background. This is because the number of $pp \rightarrow pp\eta$ events was determined for each investigated phase-space interval separately. As an example the miss-

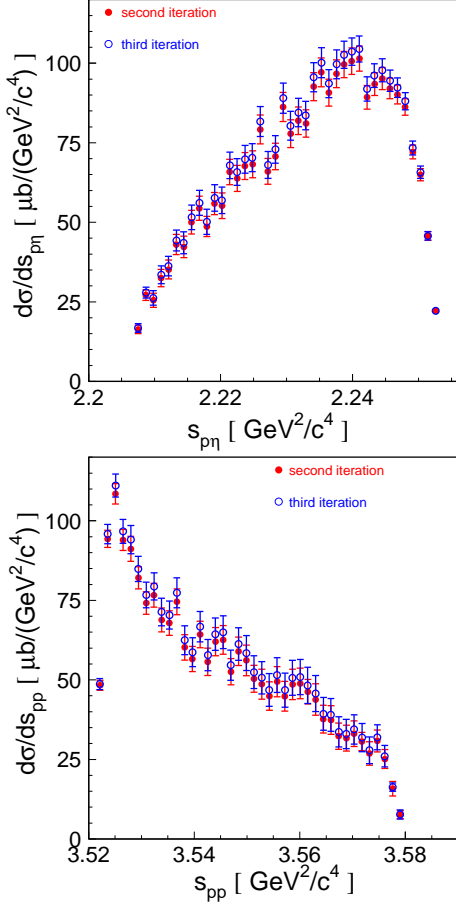


FIG. 18: Distributions of the invariant masses s_{pp} and $s_{p\eta}$ determined for the two different assumptions about the cross section dependence of the ψ angle.

ing mass spectra for three bins of the proton- η invariant mass are presented in figure 19. As already noticed for $\frac{d\sigma}{d\psi}$ the shape of the background is well reproduced locally in each region of the phase space.

C. Total and differential cross sections

Though the form of the s_{pp} , $s_{p\eta}$, and $\cos(\theta_\eta^*)$ is independent of the ψ distribution, the total cross section derived from the data depends on the shape of $\frac{d\sigma}{d\psi}$ quite significantly. It amounts to $3.24 \pm 0.03 \mu b$, yet it changes by $\pm 0.2 \mu b$ when varying the parameters of the function $\frac{d\sigma}{d\psi} = a + b \cdot |\sin(\psi)|$ by \pm three standard deviations. Therefore, we use that variation as an estimation of the systematic error in the acceptance correction. To this we must add a 3% systematical uncertainty stemming from the luminosity determination [29]. The luminosity was determined by the comparison of the measured differential distribution of the elastically scattered protons with the results of the EDDA collaboration [31]. The determined value amounts to $811 \pm 8 \pm (3\%) \text{ nb}^{-1}$. Thus the overall systematical error of the cross section value

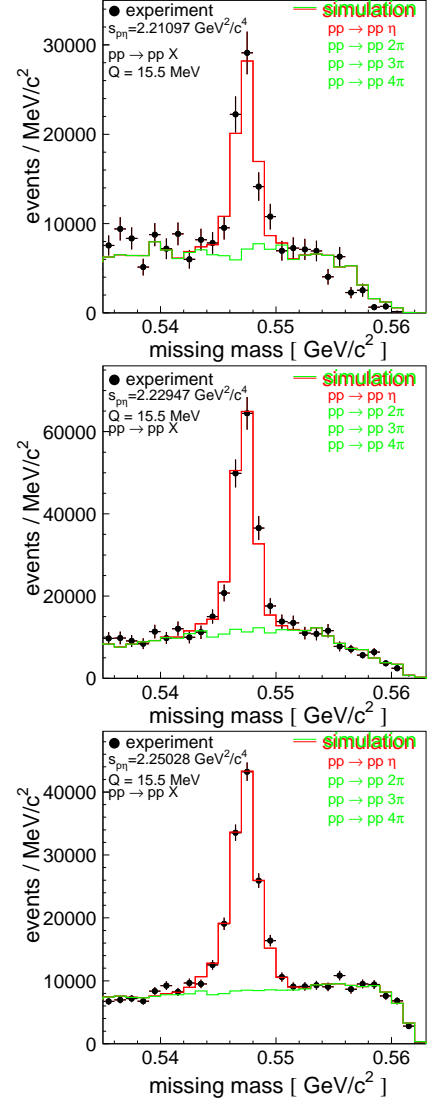


FIG. 19: Missing mass distributions determined for the invariant mass bins as depicted inside the figures. The spectra were corrected for the acceptance. The histograms show the simulations for the multi-pion background $pp \rightarrow pp(m\pi)$ and the $pp \rightarrow pp\eta$ reactions fitted to the data with the amplitudes as the only free parameters.

amounts to $0.30 \mu b$. In summary, we determined that at $Q = 15.5 \text{ MeV}$ the total cross section for the $pp \rightarrow pp\eta$ reaction is equal to $3.24 \pm 0.03 \pm 0.30 \mu b$, where the first and second error denote the statistical and systematical uncertainty, respectively [32].

In the below tables and figures we will present the values for the differential cross section concerning the observables described in section II. If possible the data will be compared to the result of measurements performed at the non-magnetic spectrometer COSY-TOF [20]. An interpretation of the elaborated distribution follows in the next section. The distributions of the squared invariant masses as presented already in figure 18, are listed in table III. The distribution of the polar angle of the η meson emission in the centre-of-mass system is given in table II

TABLE II: Differential cross section in $|\cos(\theta_\eta^*)|$, $|\cos(\theta_N^*)|$, $|\cos(\theta_{pp}^*)|$, and $|\cos(\theta_{pp}^{**})|$ for the $pp \rightarrow pp\eta$ reaction at $Q = 15.5$ MeV.

	$\frac{d\sigma}{d\Omega}(\cos(\theta_\eta^*))$ [$\frac{\mu b}{sr}$]	$\frac{d\sigma}{d\Omega}(\cos(\theta_N^*))$ [$\frac{\mu b}{sr}$]	$\frac{d\sigma}{d\Omega}(\cos(\theta_{pp}^*))$ [$\frac{\mu b}{sr}$]	$\frac{d\sigma}{d\Omega}(\cos(\theta_{pp}^{**}))$ [$\frac{\mu b}{sr}$]
.05	.259 ± .008	.216 ± .003	.256 ± .010	.276 ± .010
.15	.282 ± .009	.244 ± .004	.259 ± .010	.267 ± .010
.25	.259 ± .007	.273 ± .007	.279 ± .010	.266 ± .009
.35	.248 ± .008	.256 ± .009	.266 ± .009	.257 ± .009
.45	.253 ± .008	.288 ± .012	.251 ± .010	.255 ± .009
.55	.260 ± .008	.280 ± .014	.268 ± .009	.273 ± .008
.65	.267 ± .008	.264 ± .016	.260 ± .009	.252 ± .008
.75	.265 ± .009	.266 ± .019	.253 ± .007	.247 ± .007
.85	.249 ± .009	.237 ± .020	.245 ± .006	.259 ± .006
.95	.238 ± .011	.258 ± .021	.240 ± .003	.229 ± .004

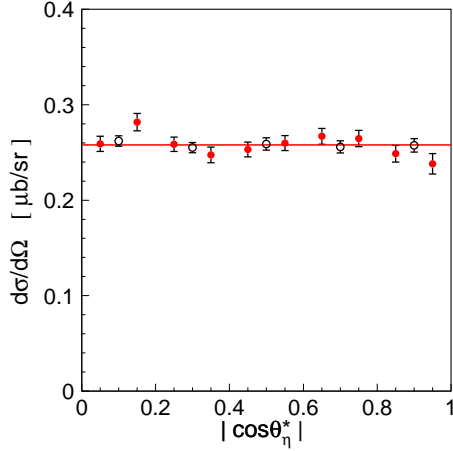


FIG. 20: Differential cross section of the $pp \rightarrow pp\eta$ reaction as a function of the η meson centre-of-mass polar angle. Full circles depict experimental results for the $pp \rightarrow pp\eta$ reaction measured at $Q = 15.5$ MeV by the COSY-11 collaboration (this article) and the open circles were determined by the TOF collaboration at $Q = 15$ MeV [20]. The TOF points were normalized in amplitude to our result, since for that data the absolute scale is not evaluated.

and shown in figure 20. Clearly, our data agree very well with the angular dependence determined by the TOF collaboration. As already mentioned, the two identical particles in the initial state of the $pp \rightarrow pp\eta$ reaction imply that the angular distribution of either ejectile must be symmetric around 90 degree in the centre-of-mass frame. Here we use that reaction characteristic, yet in the previous analysis of this data [33] we utilized this property to check the correctness of the acceptance calculation. In reference [33] we presented the differential cross section of the η meson centre-of-mass polar angle for the full range of $\cos(\theta_\eta^*)$ and found that this is completely symmetric around $\cos(\theta_\eta^*) = 0$.

For completeness we calculated also a distribution of the angle ψ_N defining the orientation of the $pp\eta$ system within the emission plane. The result is shown in figure 21 and the values of $\frac{d\sigma}{d\psi_N}$ are listed in table IV.

Up to now we presented invariant mass spectra of the

proton-proton and proton- η systems and angular distribution for two sets of non-trivial angles which describe the orientation of ejectiles within the emission plane and the alignment of the plane itself, namely $(\cos(\theta_\eta^*), \psi)$ and $(\cos(\theta_N^*), \psi_N)$.

Since one of the important issues which we will discuss in the next section is the contribution from higher partial waves we evaluated also an angular distribution of the relative momentum of two protons seen from the proton-proton centre-of-mass subsystem (see figure 22). The distribution of that angle should deliver information

TABLE III: Distribution of the square of the invariant mass of the proton-proton (s_{pp}) and proton- η ($s_{p\eta}$) systems measured at $Q = 15.5$ MeV via $pp \rightarrow pp\eta$ reaction.

s_{pp} [GeV^2/c^4]	$\frac{d\sigma}{ds_{pp}}$ [$\frac{\mu b}{GeV^2/c^4}$]	$s_{p\eta}$ [GeV^2/c^4]	$\frac{d\sigma}{ds_{p\eta}}$ [$\frac{\mu b}{GeV^2/c^4}$]
3.5221	48.7 ± 1.7	2.2075	16.8 ± 1.4
3.5236	95.8 ± 3.0	2.2087	27.9 ± 1.7
3.5251	111.1 ± 3.6	2.2098	26.2 ± 2.3
3.5265	96.7 ± 3.8	2.2110	33.5 ± 2.8
3.5280	94.1 ± 4.4	2.2121	36.2 ± 3.1
3.5294	84.9 ± 4.0	2.2133	44.3 ± 3.3
3.5309	76.7 ± 4.0	2.2144	43.6 ± 3.5
3.5324	79.4 ± 4.3	2.2156	51.6 ± 3.8
3.5338	71.3 ± 4.3	2.2168	56.1 ± 3.9
3.5353	70.4 ± 4.4	2.2179	50.2 ± 4.0
3.5367	77.4 ± 4.7	2.2191	57.6 ± 4.2
3.5382	62.5 ± 4.5	2.2202	56.9 ± 4.2
3.5397	58.7 ± 4.5	2.2214	67.9 ± 4.2
3.5411	66.7 ± 4.8	2.2225	65.8 ± 4.2
3.5426	57.8 ± 4.9	2.2237	69.8 ± 4.4
3.5440	64.4 ± 5.1	2.2248	70.3 ± 4.4
3.5455	65.0 ± 5.1	2.2260	81.7 ± 4.7
3.5469	54.6 ± 4.7	2.2272	68.0 ± 4.2
3.5484	61.3 ± 5.1	2.2283	72.9 ± 4.3
3.5499	58.4 ± 5.5	2.2295	89.0 ± 4.7
3.5513	52.4 ± 5.2	2.2306	80.3 ± 4.5
3.5528	50.7 ± 5.1	2.2318	84.5 ± 4.5
3.5542	46.8 ± 5.1	2.2329	83.6 ± 4.4
3.5557	51.5 ± 5.4	2.2341	95.6 ± 4.6
3.5572	46.8 ± 5.3	2.2353	100.2 ± 4.7
3.5586	50.7 ± 5.5	2.2364	93.6 ± 4.4
3.5601	50.9 ± 5.5	2.2376	99.7 ± 4.5
3.5615	48.3 ± 5.7	2.2387	102.6 ± 4.3
3.5630	45.7 ± 5.7	2.2399	103.6 ± 4.3
3.5645	39.3 ± 5.2	2.2410	104.5 ± 4.1
3.5659	39.0 ± 5.2	2.2422	91.9 ± 3.8
3.5674	33.6 ± 4.7	2.2433	96.1 ± 3.7
3.5688	33.0 ± 4.6	2.2445	97.8 ± 3.6
3.5703	34.4 ± 4.6	2.2457	94.5 ± 3.4
3.5718	31.8 ± 4.4	2.2468	92.3 ± 3.0
3.5732	27.9 ± 4.2	2.2480	88.1 ± 2.7
3.5747	31.9 ± 3.9	2.2491	73.3 ± 2.2
3.5761	26.0 ± 3.4	2.2503	65.7 ± 1.9
3.5776	16.3 ± 1.3	2.2514	45.7 ± 1.4
3.5790	7.7 ± 1.4	2.2526	22.2 ± 0.7

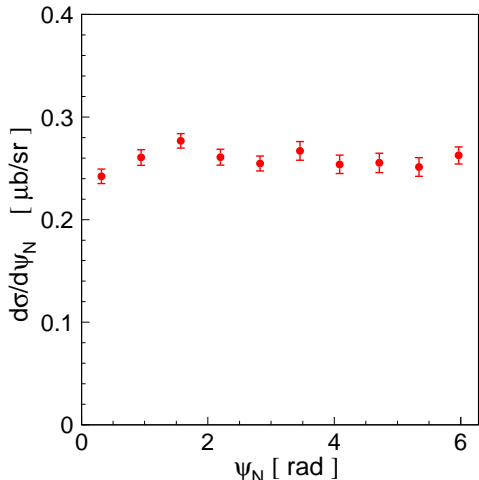


FIG. 21: Differential cross section in ψ_N for the $pp \rightarrow pp\eta$ reaction measured at $Q = 15.5$ MeV. The variable ψ_N is defined in section II.

about the partial waves of the proton-proton system in the exit channel. In case of the two body scattering, the beam line, which is at the same time the line along which the centre-of-mass system is moving, constitutes the reference frame for the angular distributions. For a three body final state the beam axis is not a good direction to look for the angular distributions relevant for the

TABLE IV: Differential cross section in ψ_N for the $pp \rightarrow pp\eta$ reaction measured at $Q = 15.5$ MeV. The variable ψ_N is defined in section II. Values are presented in figure 21.

$\psi_N [rad]$	$\frac{d\sigma}{d\psi_N} \left[\frac{\mu b}{sr} \right]$
0.314	0.242 ± 0.007
0.942	0.261 ± 0.008
1.571	0.277 ± 0.007
2.199	0.261 ± 0.008
2.827	0.255 ± 0.007
3.456	0.267 ± 0.009
4.084	0.254 ± 0.009
4.712	0.255 ± 0.009
5.341	0.251 ± 0.009
5.969	0.263 ± 0.008

relative angular momenta of the two particles [34]. But by analogy to the two body system, an instructive reference axis for angular distributions in the proton-proton subsystem is now the momentum of the recoil η meson, since the direction of that meson is identical with the direction of the movement of the proton-proton centre-of-mass subsystem. The distribution of the differential cross section in $\cos(\theta_{pp}^{**})$ is given in table II. In this table we listed also the differential cross section as a function of angle θ_{pp}^* of the relative proton momentum seen from the overall centre-of-mass frame, as this is often considered in the theoretical works. In figure 23 our results are compared to the angular distribution extracted by the TOF collaboration. Both experiments agree very well

proton-proton rest frame

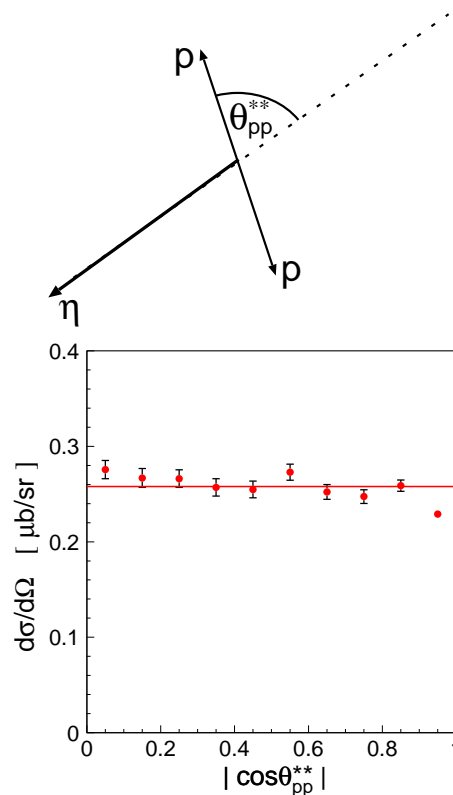


FIG. 22: Definition of θ_{pp}^{**} , the polar angle of the relative proton-proton momentum with respect to the momentum of the η meson as seen in the di-proton rest frame. Lower picture shows differential cross section in θ_{pp}^{**} as determined for the $pp \rightarrow pp\eta$ reaction at $Q = 15.5$ MeV.

within the statistical accuracy, and both indicate a slight decrease of the cross section with increasing $|\cos(\theta_{pp}^*)|$.

IV. INTERPRETATION OF RESULTS

The interaction between particles depends on their relative momenta or equivalently on the invariant masses of the two-particle subsystems. Therefore it should show up as modification of the phase-space abundance in the kinematical regions where the outgoing particles possess small relative velocities. Only two invariant masses of the three subsystems are independent and therefore the entire accessible information about the final state interaction of the three-particle system can be presented in the form of the Dalitz plot. The upper panel of figure 24 indicates the event distribution as determined experimentally for the $pp\eta$ system at an excess energy of $Q = 15.5$ MeV. In this figure one easily recognizes the growths of the population density at the region where the protons have small relative momenta which can be assigned to the strong attractive S-wave interaction between the two protons. This is qualitatively in agreement with the expectation presented in figure 24(middle), which shows the results of Monte-Carlo calculations where the homo-

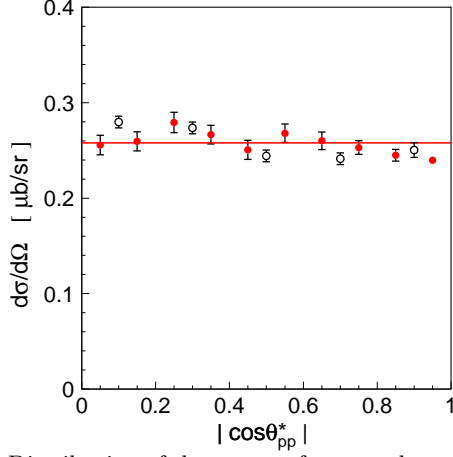


FIG. 23: Distribution of the centre-of-mass polar angle of the relative protons momentum with respect to the beam direction determined for the $pp \rightarrow pp\eta$ reaction at $Q = 15.5$ MeV. The COSY-11 result (closed circles) is compared to the data points determined at $Q = 15$ MeV by the TOF collaboration (open circles) [20].

generously populated phase space was weighted by the square of the on-shell 1S_0 proton-proton scattering amplitude. However, already in this two dimensional representation it is visible that the experimentally determined distribution remains rather homogeneous outside the region of the small proton-proton invariant masses, whereas the simulated abundance decreases gradually with growing s_{pp} (as indicated by the arrow). The lower panel of figure 24 shows the simulated phase-space density distribution disregarding the proton-proton interaction but accounting for the interaction between the η -meson and the proton. Due to the lower strength of this interaction the expected deviations from a uniform distribution is smaller by about two orders of magnitude, yet an enhancement of the density in the range of low invariant masses of proton- η subsystems is clearly visible. Note that the scale in the lower figure is linear whereas in the middle and upper panel it is logarithmic. Due to weak variations of the proton- η scattering amplitude the enhancement originating from the η -meson interaction with one proton is not separated from the η -meson interaction with the second proton. Therefore an overlapping of broad structures occurs. It is observed that the occupation density grows slowly with increasing s_{pp} , opposite to the effects caused by the S-wave proton-proton interaction, but similar to the modifications expected for the NN P-wave [35]. From the above example it is obvious that, only from experiments with high statistics, signals of the meson-nucleon interaction can be observed over the overwhelming nucleon-nucleon final state interaction. A deviation of the experimentally observed population of the phase-space from the expectation based on the mentioned assumptions is even better visible in figure 25. This figure presents the projection of the phase-space distribution onto the s_{pp} axis corresponding to the axis indicated by the arrows in the two lower parts of figure 24. The super-

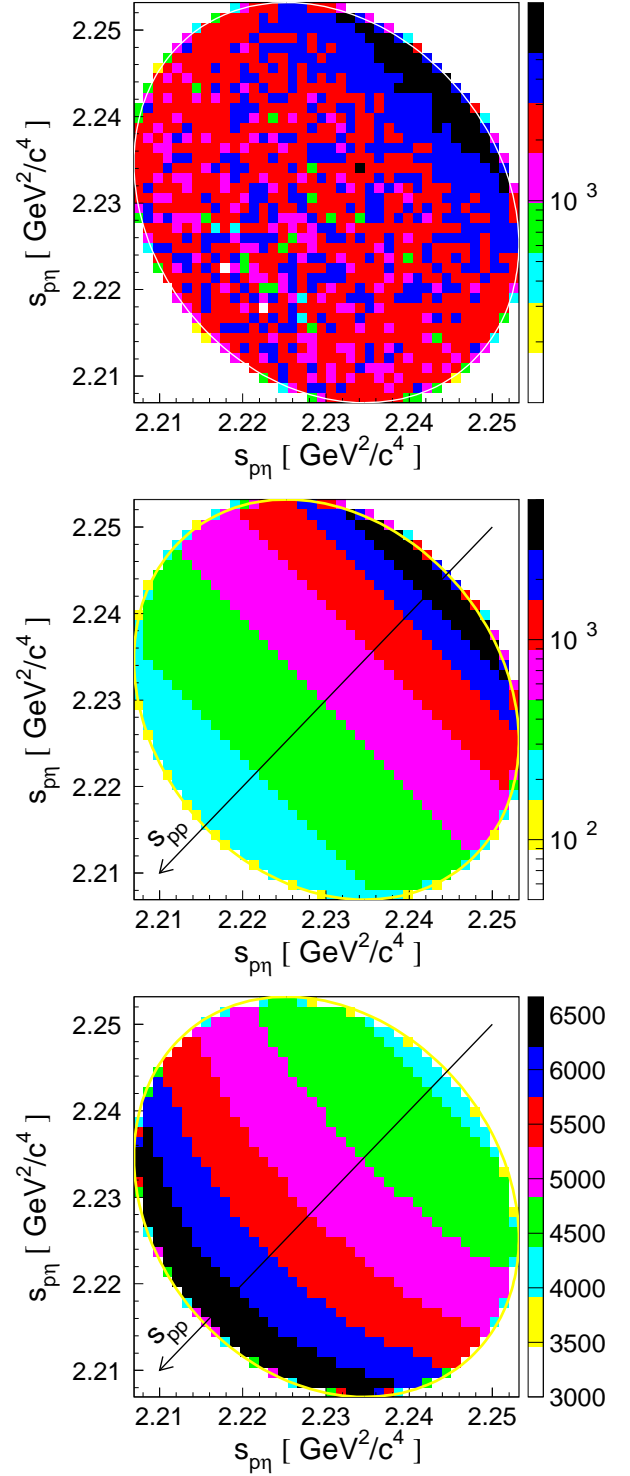


FIG. 24: Dalitz plot distributions.

(upper panel) Experimental result determined for the $pp \rightarrow pp\eta$ reaction at $Q = 15.5$ MeV. Data were corrected for the detection acceptance and efficiency.

(middle) Monte-Carlo simulations for the $pp \rightarrow pp\eta$ reaction at $Q = 15.5$ MeV: Phase-space density distribution modified by the 1S_0 proton - proton final state interaction.

(lower panel) Simulated phase-space density distribution modified by the proton- η interaction with a scattering length of $a_{p\eta} = 0.7 \text{ fm} + i 0.3 \text{ fm}$. Details of the calculations together with the discussion of the nucleon-nucleon and nucleon-meson final state interaction can be found in reference [14].

The scale in the figure is linear in contrast to the above panels. Lines surrounding the plots show the kinematical limits.

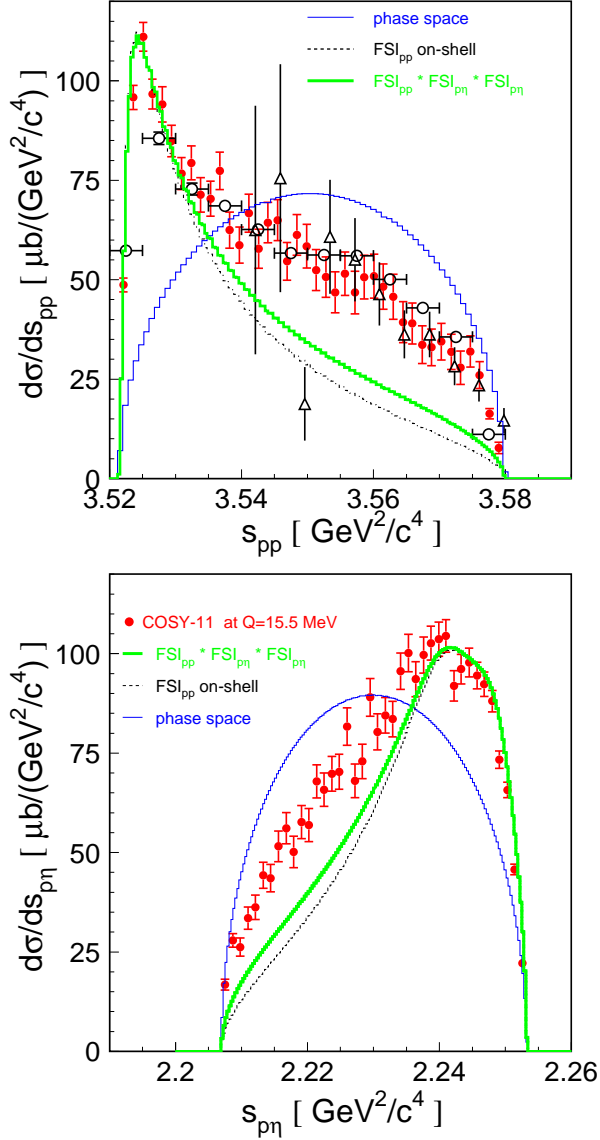


FIG. 25: Distributions of the square of the proton-proton (s_{pp}) and proton- η ($s_{p\eta}$) invariant masses determined experimentally for the $pp \rightarrow pp\eta$ reaction at the excess energy of $Q = 15.5$ MeV by the COSY-11 collaboration (closed circles), at $Q = 15$ MeV by TOF collaboration (open circles) [20], and at $Q = 16$ MeV by PROMICE/WASA (open triangles) [37]. The TOF and PROMICE/WASA data have been normalized to those of COSY-11, since these measurements did not evaluate the luminosities but rather normalized the results to reference [5] (see also comment [32]). The integrals of the phase space weighted by the square of the proton-proton on-shell scattering amplitude (dotted lines)– FSI_{pp} , and by the product of FSI_{pp} and the square of the proton- η scattering amplitude (thick solid lines), have been normalized arbitrarily at small values of s_{pp} . The thick solid line was obtained assuming a scattering length of $a_{p\eta} = 0.7 \text{ fm} + i 0.4 \text{ fm}$. The expectation under the assumption of the homogeneously populated phase space are shown as thin solid curves.

imposed lines in figure 25 correspond to the calculations performed under the assumption that the production amplitude can be factorized into a primary production and final state interaction. The dotted lines result from calculations where only the proton-proton FSI was taken into account, whereas the thick-solid lines present results where the overall enhancement was factorized into the corresponding pair interactions of the $pp\eta$ system. This factorisation Ansatz is of course only valid if the different amplitudes are completely decoupled which is certainly not the case here. Therefore, this calculations should be considered as a rough estimate of the effect introduced by the FSI in the different two body systems. The enhancement factor accounting for the proton-proton FSI has been calculated [14, 38] as the square of the on-shell proton-proton scattering amplitude derived according to the modified Cini-Fubini-Stanghellini formula including the Wong-Noyes Coulomb corrections [39]. The homogeneous phase-space distribution (thin solid lines) deviate strongly from the experimentally determined spectra. The curves including the proton-proton and proton- η FSI reflect the shape of the data for small invariant masses of the proton-proton system, yet they deviate significantly for large s_{pp} and small $s_{p\eta}$ values. An explanation for this discrepancy could be a contribution from P-wave proton-proton interaction [11], or a possibly inadequate assumption that proton- η and proton-proton interaction modify the phase space occupations only as incoherent weights [36].

Slightly better description is achieved when the proton-proton interaction is accounted for by the realistic nucleon-nucleon potential. The upper picture in figure 26 depicts the results obtained using two different models for the production process as well as for the NN interaction [10, 41] [11, 42]. The calculations for the ${}^3P_0 \rightarrow {}^1S_0 s$ transition differ slightly, but the differences between the models are, by far, smaller than the observed signal.

Therefore we can safely claim that the discussed effect is rather too large to be caused by the particular assumptions used for the production operator and NN potential.

As can be seen in figure 20, the distribution of the η polar angle in the center of mass frame is fully isotropic. This is the next evidence — besides the shape of the excitation function and the kinematical arguments discussed in reference [14] — that at this excess energy ($Q = 15.5$ MeV) the η meson is produced in the center of mass frame predominantly with the angular momentum equal to zero. Similarly, the distribution determined for the polar angle of the relative proton-proton momentum with respect to the momentum of the η meson as seen in the di-proton rest frame is also consistent with isotropy. Anyhow, even the isotropic distribution in this angle does not imply directly that the relative angular momentum between protons is equal to zero, because of their internal spin equal to $\frac{1}{2}$. Therefore, the contribution from the 3P_0 -wave produced via the ${}^1S_0 \rightarrow {}^3P_0 s$ transition cannot be excluded. The isotropic angular distribution, as pointed out in reference [11], can also be prin-

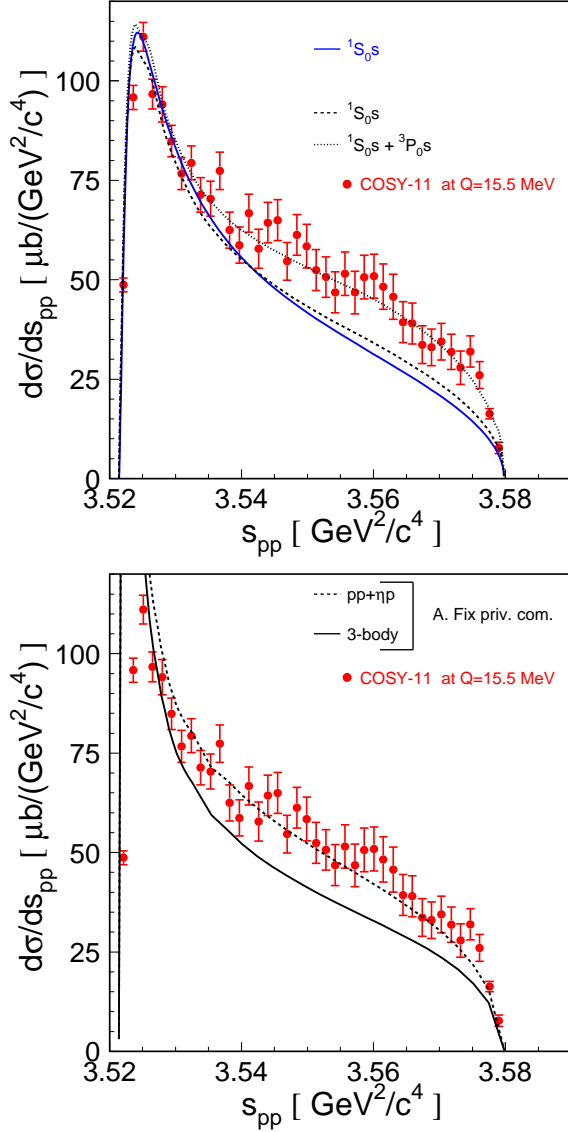


FIG. 26: **(upper picture)** Distribution of the square of the proton-proton (s_{pp}) invariant mass for the $pp \rightarrow pp\eta$ reaction at an excess energy of $Q = 15.5$ MeV. Solid and dashed lines corresponds to the calculations under the assumption of the ${}^3P_0 \rightarrow {}^1S_0s$ transition according to the models described in references [10, 41] and [11, 42], respectively. The dotted curve shows the result with the inclusion of the ${}^1S_0 \rightarrow {}^3P_0s$ contribution as suggested in reference [11].

(lower picture) The same data as above but with curves denoting preliminary three-body calculations [18] of the final $pp\eta$ system as described in [40]. At present only the dominant transition ${}^3P_0 \rightarrow {}^1S_0s$ is taken into account and the production mechanism is reduced to the excitation of the $S_{11}(1535)$ resonance via the exchange of the π and η mesons. The solid line was determined with the rigorous three-body approach [18] where the proton-proton sector is described in terms of the separable Paris potential (PEST3) [43], and for the η -nucleon scattering amplitude an isobar model analogous to the one of reference [44] is used with $a_{\eta N} = 0.5 \text{ fm} + i \cdot 0.32 \text{ fm}$. The dashed line is obtained if only pairwise interactions ($pp + p\eta$) are allowed. The effect of proton-proton FSI at small s_{pp} is overestimated due to neglect of Coulomb repulsion between the protons. The lines are normalized arbitrarily but their relative amplitude is fixed from the model.

TABLE V: Square of the proton-proton invariant mass from the $pp \rightarrow pp\eta$ reaction measured for the excess energy range $4 \text{ MeV} \leq Q \leq 5 \text{ MeV}$ [6, 46].

$s_{pp} [\text{GeV}^2/c^4]$	$\frac{d\sigma}{ds_{pp}} \left[\frac{\mu\text{b}}{\text{GeV}^2/c^4} \right]$
3.52164	19.0 ± 13
3.52204	74.0 ± 21
3.52264	56.9 ± 15
3.52344	91.7 ± 17
3.52444	69.8 ± 13
3.52564	56.9 ± 11
3.52704	51.2 ± 9.9
3.52864	41.8 ± 8.4
3.53044	43.4 ± 8.1
3.53244	36.6 ± 7.0
3.53464	24.7 ± 5.5
3.53704	6.8 ± 2.8
3.53964	1.1 ± 1.1

cially achieved by the destructive interference between the transitions ${}^1S_0 \rightarrow {}^3P_0s$ and ${}^1D_2 \rightarrow {}^3P_2s$.

As show in reference [11] the invariant mass distributions can be very well described when including higher partial-wave amplitudes. In fact, as depicted by the dotted line in the upper panel of figure 26, an admixture of the ${}^1S_0 \rightarrow {}^3P_0s$ transition leads to the excellent agreement with the experimentally determined invariant mass spectra. However, at the same time, the model of reference [11] leads to strong discrepancies in the shape of the excitation function as can be deduced from the comparison of the dashed-dotted line and the data in figure 1. Whereas it describes the data points in the excess energy range between 40 MeV and 100 MeV it underestimates the total cross section below 20 MeV by a factor of 2.

Interestingly, the enhancement at large s_{pp} is visible also at much lower excess energy. This can be concluded from figure 27 in which the COSY-11 data at $Q \approx 4.5$ MeV [46] are compared to the simulations based on the assumption that the phase-space abundance is due to the proton-proton FSI only. This observation could imply that the effect is caused by the proton- η interaction rather than higher partial waves, since their contribution at such small energies is quite improbable [14]. However, as shown in the lower part of figure 26 the rigorous three-body treatment of the $pp\eta$ system leads at large values of s_{pp} to the reduction of the cross section in comparison to the calculation taking into account only first order rescattering ($pp + p\eta$) [18]. Here, both calculations include only the ${}^3P_0 \rightarrow {}^1S_0s$ transition. Though the presented curves are still preliminary, we can qualitatively assess that the rigorous three-body approach, in comparison to the present estimations, will on the one hand enhance the total cross section near threshold as shown in figure 1, while on the other hand it will decrease the differential cross section at large values of s_{pp} . This is just opposite to the influence of P-waves in the proton-proton system.

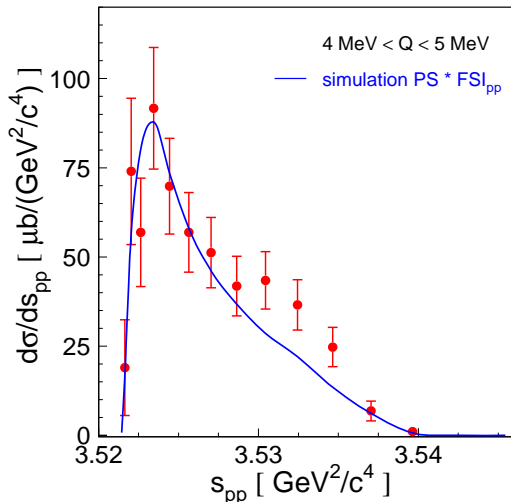


FIG. 27: Distribution of square of the proton-proton invariant mass from the $pp \rightarrow pp\eta$ reaction measured at COSY-11 for the excess energy range $4 \text{ MeV} \leq Q \leq 5 \text{ MeV}$ [6, 46]. Numerical values are listed in table V. The superimposed line shows the result of simulations performed under the assumption that the phase space population is determined exclusively by the on-shell interaction between outgoing protons. The "tail" at large s_{pp} values is due to the smearing of the excess energy, since this former COSY-11 data have not been kinematically fitted. Additionally to the 1 MeV range of Q a smearing of about 0.3 MeV (σ) should be taken into account.

From the above presented considerations it is rather obvious that the rigorous three-body treatment of the produced $pp\eta$ system and the exact determination of the contributions from the higher partial waves may result in the simultaneous explanation of both observations: the near-threshold enhancement of the excitation function of the total cross section, and the strong increase of the invariant mass distribution at large values of s_{pp} . For the unambiguous determination of the contributions from different partial waves spin dependent observables are required [11]. The first attempt has been already reported in [45].

V. CONCLUSION

Using the stochastically cooled proton beam at the Cooler Synchrotron COSY and the COSY-11 facility

we have determined the total and differential cross sections for the $pp \rightarrow pp\eta$ reaction at an excess energy of $Q = 15.5 \text{ MeV}$. The high statistics data sample allowed us for the clear separation of events corresponding to the $pp \rightarrow pp\eta$ reaction from the multi-pion production at each investigated phase-space bin, and the multidimensional acceptance correction allowed to extract the result without necessity of any assumption about the reaction process.

The determined distributions of the centre-of-mass polar angle of the η meson emission as well as the distribution of the relative proton-proton momentum with respect to the momentum of the η meson are consistent with isotropy. Though, in the latter a small tendency of an increase of the cross section at 90 degree is observed. In contrary a rather strong decrease of the cross section was found at 90 degree for the center-of-mass polar angle of the vector normal to the emission plane. Explanation of that effect may reveal an interesting characteristic of the dynamics of the production process.

The determined invariant mass spectra of the two-particle subsystems deviate strongly from the predictions based on the homogenous population of events over the phase space. Deviations at low proton-proton invariant mass values can be well explained as an influence of the S-wave interaction between the two protons. However, an unexpectedly large enhancement of the occupation density in the kinematical regions of low η -proton relative momentum is not yet understood. We have demonstrated that for the simultaneous description of the excitation function and invariant mass distributions a rigorous three-body calculation with inclusion of the contribution from higher partial waves is needed.

Acknowledgments

We acknowledge the stimulating discussions and help of V. Baru, A. Fix and Ch. Hanhart. The work has been partly supported by the European Community - Access to Research Infrastructure action of the Improving Human Potential Programme as well as the Internationales Büro and the Verbundforschung of the BMBF, and by the Polish State Committee for Scientific Research (grant: 2P03B07123).

-
- [1] F. Balestra et al., Phys. Lett. **B 491**, 29 (2000);
R. Wurzinger et al., Phys. Lett. **B 374**, 283 (1996);
P. Moskal et al., Phys. Lett. **B 474**, 416 (2000);
P. Moskal et al., Phys. Rev. Lett. **80**, 3202 (1998);
A. Khoukaz et al., Ann. Rep., IKP Uni. Münster (2001).
 - [2] F. Hibou et al., Phys. Lett. **B 438**, 41 (1998).
 - [3] E. Chiavassa et al., Phys. Lett. **B 322**, 270 (1994);
H. Calén et al., Phys. Rev. Lett. **79**, 2642 (1997).
 - [4] A. M. Bergdolt et al., Phys. Rev. **D 48**, R2969 (1993).
 - [5] H. Calén et al., Phys. Lett. **B 366**, 39 (1996).
 - [6] J. Smyrski et al., Phys. Lett. **B 474**, 182 (2000).
 - [7] H. O. Meyer et al., Nucl. Phys. **A 539**, 633 (1992);
A. Bondar et al., Phys. Lett. **B 356**, 8 (1995);
J. Greiff et al., Phys. Rev. **C 62**, 064002 (2000);
M. Betigeri et al., Nucl. Phys. **A 690**, 473 (2001);
D. A. Hutcheon et al., Phys. Rev. Lett. **64**, 176 (1990).
 - [8] H. O. Meyer et al., Phys. Rev. **C 63**, 064002 (2001).
 - [9] M. Batinić et al., Phys. Scripta **56**, 321 (1997);

- A. Moalem et al., Nucl. Phys. **A 600**, 445 (1996);
 J.F. Germond, C. Wilkin, Nucl. Phys. **A 518**, 308 (1990);
 J.M. Laget et al., Phys. Lett. **B 257**, 254 (1991);
 T. Vetter et al., Phys. Lett. **B 263**, 153 (1991);
 B.L. Alvaredo, E. Oset, Phys. Lett. **B 324**, 125 (1994);
 M.T. Peña et al., Nucl. Phys. **A 683**, 322 (2001);
 F. Kleefeld, M. Dillig, Acta Phys. Polon. **B 29**, 3059 (1998);
 S. Ceci, A. Švarc, e-Print Archive: nucl-th/0301036.
- [10] V. Baru et al., Phys. Rev. **C 67**, 024002 (2003).
 [11] K. Nakayama et al., e-Print Archive: nucl-th/0302061.
 [12] K. Nakayama et al., Phys. Rev. **C 61**, 024001 (1999);
 E. Gedalin et al., Nucl. Phys. **A 650**, 471 (1999);
 V. Baru et al., Eur. Phys. J. **A 6**, 445 (1999);
 S. Bass, Phys. Lett. **B 463**, 286 (1999);
 A. Sibirtsev, W. Cassing, Eur. Phys. J. **A 2**, 333 (1998).
 [13] V. Bernard, N. Kaiser, Ulf-G. Meißner, Eur. Phys. J. **A 4**, 259 (1999).
 [14] P. Moskal, M. Wolke, A. Khoukaz, W. Oelert, Prog. Part. Nucl. Phys. **49**, 1 (2002).
 [15] G. Fäldt, T. Johansson, C. Wilkin, Physica Scripta **T 99**, 146 (2002).
 [16] H. Machner et al., J. Phys. **G 25**, R231 (1999).
 [17] A. M. Green, S. Wycech, Phys. Rev. **C 55**, R2167 (1997).
 [18] A. Fix, H. Arenhövel, in preparation (2003).
 [19] V. Hejny et al., Eur. Phys. J. **A 13**, 493 (2002);
 Ch. Elster et al., e-Print Archive: nucl-th/0207052;
 A. Sibirtsev et al., Phys. Rev. **C 65** 067002, (2002).
 [20] M. Abdel-Bary et al., Eur. Phys. J. **A 16**, 127 (2003).
 [21] U. Schubert, PhD thesis, University of Uppsala, Acta Universitatis Upsaliensis **5** (1995).
 [22] S. Brauksiepe et al., Nucl. Instr. & Meth. **A 376**, 397 (1996).
 [23] P. Moskal et al, Nucl. Instr. & Meth **A 466**, 448 (2001).
 [24] D. Prasuhn et al., Nucl. Instr. & Meth. **A 441**, 167 (2000).
 [25] F. Balestra et al., Phys. Rev. Lett. **89**, 092001 (2002).
 [26] J. Ritman, Habilitation thesis, Gießen University (2000).
 [27] E. Roderburg et al., Acta Phys. Pol. **B 31**, 2299 (2000).
 [28] H. Dombrowski et al., Nucl. Instr. & Meth. **A 386**, 228 (1997).
 [29] P. Moskal, PhD thesis, Jagellonian University, Cracow (1998).
 [30] K. Hagiwara et al., Phys. Rev. **D 66**, 010001 (2002).
 [31] D. Albers et al., Phys. Rev. Lett. **78**, 1652 (1997).
 [32] The WASA/PROMICE collaboration determined the total cross section of 2.11 ± 0.74 (overall error) at $Q = 15.0 \pm 0.5$ MeV [5]. This value is by about 30% lower than our result, though the values still agree with each other if one adds the statistical and systematical uncertainties. However, the acceptance correction for this experiment was calculated taking into account the phase space distribution only [21] and this lead to the underestimation of the total cross section which can be deduced from the comparison between the s_{pp} distribution and the phase space prediction shown in figure 25. For the discussion of that issue see also [47]. Our result agrees, however, quite well with that of the SPES III collaboration ($3.46 \pm 0.69 \mu b$ at $Q = 16 \pm 0.6$ MeV) [4] and the reanalysis of this data reported in reference [2] which gave $2.68 \pm 0.54 \mu b$.
 [33] P. Moskal et al., πN Newsletter **16**, 367 (2002).
 [34] D. Grzonka, K. Kilian, Proceedings of the Symp. on Threshold Meson Production in pp and pd Interactions, June 20-24, 2001, Cracow, Poland; Eds. P. Moskal and M. Wolke, Schriften des FZ-Jülich Matter & Materials **11**, 100 (2002).
 [35] J. Dyring, Ph.D. thesis, University of Uppsala, Acta Universitatis Upsaliensis **14** (1997).
 [36] For the discussion of the FSI effects see eg.: F. Kleefeld, e-Print Archive nucl-th/0108064; Proceedings of the Symp. on Threshold Meson Production in pp and pd Interactions, June 20-24, 2001, Cracow, Poland; Eds. P. Moskal and M. Wolke, Schriften des FZ-Jülich Matter & Materials **11**, 51 (2002).
 [37] H. Calén et al., Phys. Lett. **B 458**, 190 (1999).
 [38] P. Moskal et al., Phys. Lett. **B 482**, 356 (2000).
 [39] H. P. Noyes, H. M. Lipinski, Phys. Rev. **C 4**, 995 (1971).
 [40] A. Fix, H. Arenhövel, Nucl. Phys. **A 697**, 277 (2002).
 [41] V. Baru, private communication (2003).
 [42] Here the model described in [11] was improved and the Coulomb interaction between protons was taken into account.
 [43] J. Haidenbauer, W. Plessas, Phys. Rev. **C 30**, 1822 (1984).
 [44] C. Bennhold, H. Tanabe, Nucl. Phys. **A 530**, 625 (1991).
 [45] P. Winter et al., Phys. Lett. **B 544**, 251 (2002); Erratum-ibid. **B 553**, 339 (2003).
 [46] J. Smyrski, P. Wüstner et al., Ann. Rep. IKP FZ-Jülich, Jül-3640 39, (1999).
 [47] S. AbdEl Samad et al., e-Print Archive: nucl-ex/0212024.